Fluid-structure coupling in the guide vanes cascade of a pump-turbine scale model

2010 IOP Conf. Ser.: Earth Environ. Sci. 12 012074

(http://iopscience.iop.org/1755-1315/12/1/012074)

IOP Conf. Series: Earth and Environmental Science **12** (2010) 012074 doi:10.1088/1755-1315/12/1/012074

Fluid-structure coupling in the guide vanes cascade of a pump-turbine scale model

S Roth[1], V Hasmatuchi[1], F Botero[1], M Farhat[1] and F Avellan[1]

[1]Laboratory for Hydraulic Machines, Ecole Polytechnique Fédérale de Lausanne
Av. de Cour 33bis, Lausanne, 1007, Switzerland

E-mail: steven.roth@epfl.ch

Abstract. The present study concerns fluid-structure coupling phenomena occurring in a guide vane cascade of a pump-turbine scale model placed in the EPFL PF3 test rig. An advanced instrument set is used to monitor both vibrating structures and the surrounding flow. The paper highlights the interaction between vibrating guide vanes and the flow behavior. The pressure fluctuations in the stay vanes region are found to be strongly influenced by the amplitude of the vibrating guide vanes. Moreover, the flow induces different hydrodynamic damping on the vibrating guide vanes depending on the operating point of the pump-turbine.

1. Introduction

Pump-turbines guide vanes cascade undergoes fluid-structure coupling phenomena. The nowadays development of new distributor type, where each guide vane is controlled independently with individual servomotor (see Bouschon et al. [1]), imposes the knowledge of the dynamic behavior of such blades placed in cascade. The transfer function characterizing each of the servomotors must account for neighboring vibrating blades as well as for the surrounding flow to ensure safety and reliability. Moreover, the case of an emergency occurring when a guide vane safety shear pin breaks inducing a guide vane to flutter in the cascade is a situation in which the overall dynamic of the guide vanes cascade may strongly be modified. The understanding of the fluid-structure coupling in the guide vanes cascade constitutes, thus, a great challenge in ensuring reliability of hydraulic pump-turbines.

In the domain of axial gas turbomachines, the slender shape of blades has forced the scientists to already look, some decades ago, into fluid-structure coupling phenomena such as flutter. Structural mistuning of bladed-disk accounting or not for asymmetric aerodynamic forces is investigated respectively by Miyakozawa et al. [2] and Yan et al. [3]. In such turbomachines, influence of neighboring guide vanes is modeled as a stiffness matrix with non-diagonal components in governing equations. Nevertheless, in hydraulic turbomachines, strong inertial and damping effects mainly due to fluid density complicate the blades dynamics. Knowledge on added mass and hydrodynamic damping is the key issue for having a reliable model. Added mass has widely been tackled for bluff bodies (e.g. Brennen [4]). Experimentally, hydrodynamic damping has been verified by Kaminer and Kavitskii [5] to vary linearly with the surrounding flow velocity as already proven analytically by Theodorsen [6]. The hydrodynamic damping issue was experimentally investigated by Roth et al. [7] in the case of a cantilever blade placed in the EPFL High Speed Cavitation Tunnel in the Laboratory for Hydraulic Machines in Lausanne. Bending eigen mode hydrodynamic damping was found to vary linearly with the flow velocity. The effect of flow velocity was strong for the bending natural mode whereas no effect of the flow velocity was observed for the torsion eigen mode hydrodynamic damping for the reduced flow velocity range investigated. Recently, Münch et al. [8] developed a numerical model to study hydro-elastic behavior of vibrating blades and looked in particular into damping forces acting on immersed blades. Finally, since the present paper focuses on the guide vanes vibrations induced by the rotor-stator interaction, information about this phenomenon in pump-turbines is given by Zobeiri et al. [9].

The present paper begins with the description of the case study. An overview of the experimental setup is then given. The results are presented in two distinct parts: the flow influence on structure vibrations is treated, and then, the structure vibrations influence on flow behavior is investigated. A final discussion concludes the paper.

2. Case study

The case study consists of three adjacent blades, voluntary weakened at their shaft level (see Fig. 1) and placed in an overall guide vanes cascade of a $\nu = 0.19$ specific speed pump-turbine scale model (see Fig. 2). The impeller features 9 blades and 20 guide vanes. The weakening of the three guide vanes induces higher vibration amplitude, strengthening in this way the fluid-structure coupling. The weakened guide vanes can be completely decoupled from the overall cascade as the other guide vanes are much stiffer. The guide vane opening angle is set to 18°. The guide vanes are made of bronze CuSn12 ($E = 90-110$ GPa, $\sigma_{elastic} = 140$ MPa, $\rho = 8'300$ kg/m^3). Two guide vanes arrangements are used (see Fig. 2) : configuration 1 (a) and 2 (b).

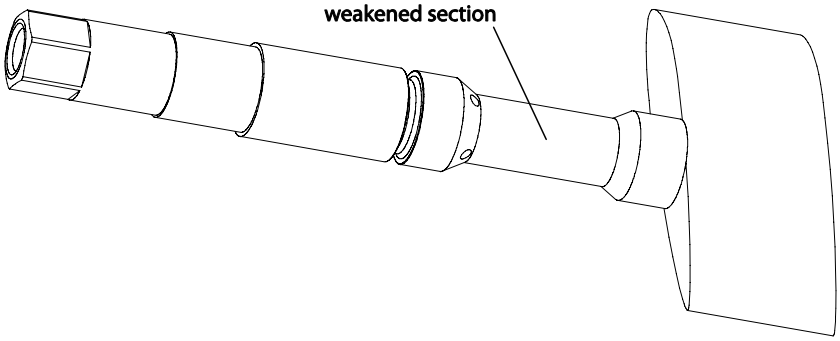

Fig. 1 Weakened guide vane

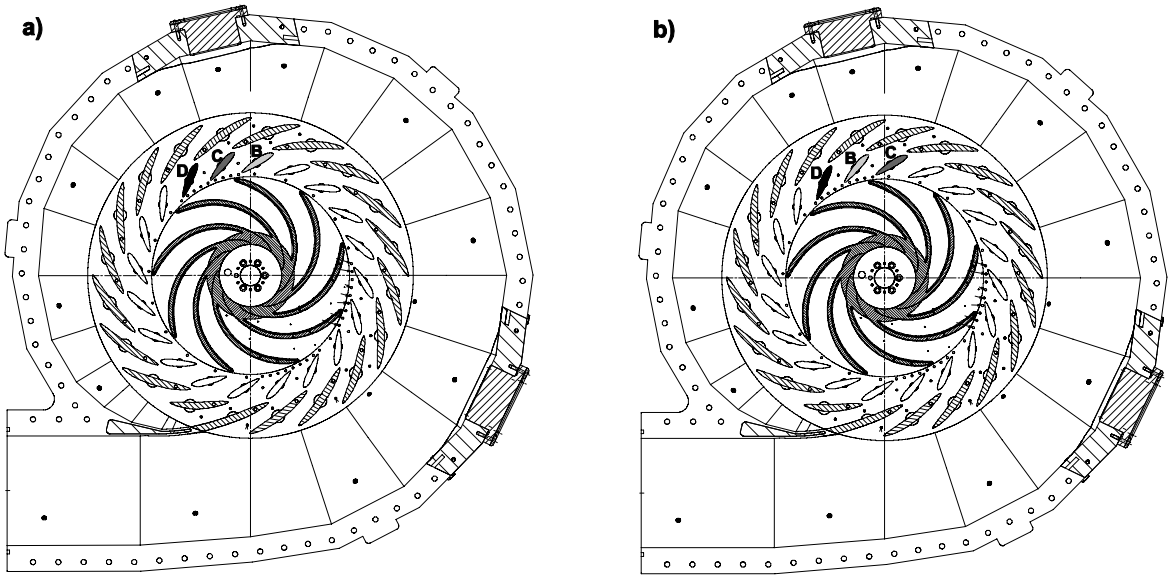

Fig. 2 Two weakened guide vanes arrangements: (a) configuration 1; (b) configuration 2

3. Experimental setup

The pump-turbine scale model is placed in the EPFL PF3 test rig. The test rig features 100 m maximum head, 1.4 m^3 maximum discharge and 1500 rpm maximum speed. An advanced instrument set is installed in the pump-turbine to measure fluid-structure coupling phenomena in the most reliable manner. Roth et al. [10] describes the set of instrument in detail. The aim of the present paper being not to describe completely the instrument set once

again, a short summary of the experimental setup is nevertheless given to satisfy those who are interested in having a rapid overview.

Two Piezo-resistive strain gages full Wheatstone bridges are installed on the weakened section of each of the three guide vanes in order to monitor bending and torsion. The sensors are calibrated statically in terms of bending force and torsion torque. The relative fluctuating bending force F' is given as follows.

$$F' = \frac{F - \bar{F}}{\bar{F}} \tag{1}$$

where F is the bending force (see Fig. 3) and $\bar{F}$, the bending force time average.

Since the calibration has been carried out statically, the relative fluctuating bending force is equivalent to the relative fluctuating bending motion as shown in equation (2).

$$y' = \frac{y - \bar{y}}{\bar{y}} = \frac{F/K - \bar{F}/K}{\bar{F}/K} = F' \quad , \tag{2}$$

where y denotes the bending displacement defined positive in the direction providing an increase of the attack angle (see Fig. 3), $\bar{y}$ the bending motion time average and K the bending stiffness.

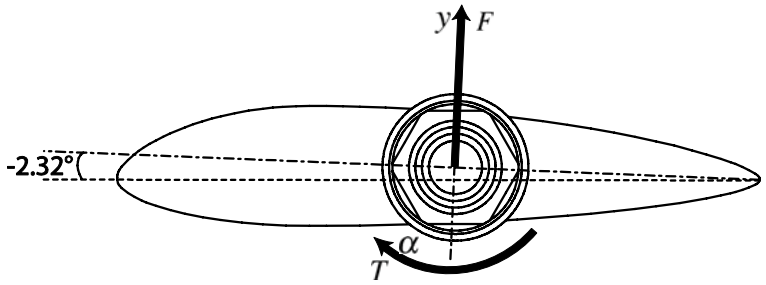

Fig. 3 Bending force/displacement and torque/rotation direction

Twenty-nine piezo-resistive pressure sensors are flush mounted in the upper flange in the pump-turbine stator mainly around the weakened guide vanes. In the present study, four sensors are of interest. They are situated in the inter-stay vanes space upstream from the weakened guide vanes (see Fig. 4). The pressure sensors are calibrated statically up to 6 bar. The pressure coefficient $\tilde{C}_p$ used in the following lines is defined as follows:

$$\tilde{C}_p = \frac{p - \bar{p}}{\rho \cdot E} \tag{3}$$

where ρ is the water density, E the specific energy of the pump-turbine related to the operating point, p the pressure and finally $\bar{p}$ the pressure time average.

A Dytran 5850B hammer is used to give an impulse excitation in air. In water, a non-intrusive system is used to create an impulse excitation (see Pereira et al. [11]). A spark plug is, thus, flush mounted in the bottom flange in the inter-guide vanes space. Two locations SP1 and SP2 (see Fig. 4) are possible. Strong shock waves travel towards the blades providing an impulse excitation. The shock waves are due to the rapid growing of a vapor bubble produced by the discharge of a capacitor.

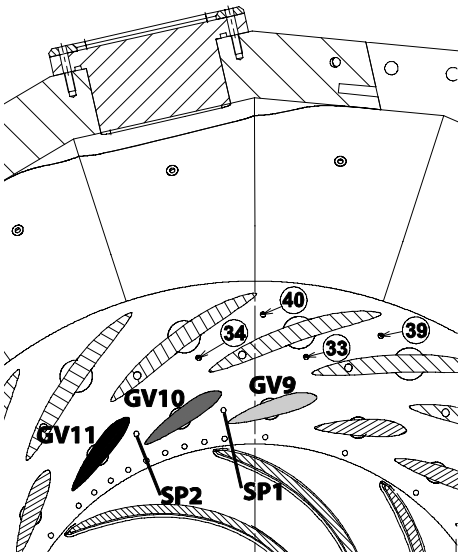

Fig. 4 Pressure sensors (33, 34, 39 & 40), spark plug (SP1 & SP2) and guide vanes (GV9, GV10 & GV11) locations

4. Results

4.1. Structural vibration influence on flow behavior

The surrounding fluid is strongly influenced by vibrating structures. Due to incompressibility, higher amplitude of the guide vane vibration induces stronger pressure fluctuation in the proximity of the vibrating structure. Roth et al. [10] showed this phenomenon in the vaneless gap between the stator and the rotor. In the stay vanes, the same occurs upstream from the vibrating guide vanes. The same operating points as used in Roth et al. [10] are chosen in order to be as consistent as possible. The discharge coefficient, energy coefficient and the impeller blade passage frequency of the operating points are given in Tab. 1.

Tab. 1 Specifications of the operating points OP#1 to OP#3

	Units	**OP#1**	**OP#2**	**OP#3**
ϕ	[-]	0.361	0.361	0.361
ψ	[-]	5.429	5.429	5.429
f_p	[Hz]	147.0	112.5	128.0

The discharge and energy coefficients are kept constant. By varying the impeller rotational speed, two cases of guide vanes resonance (OP#2 – bending mode at 225 Hz and OP#3 – bending mode at 256 Hz) and one out-of-resonance case (OP#1) are reached. In the two former cases, the 1st harmonic of the rotor-stator interaction (RSI) excites the 1st natural bending mode of the guide vanes (see Fig. 6 and Fig. 7 respectively for OP#2 and OP#3). In the latter case, no guide vane resonance is reached since the impeller passage frequency is far from the guide vane natural frequencies (see Fig. 5). Quantitatively, in resonance cases, the three guide vanes respond with a higher amplitude, but depending on the operating point or the impeller rotation speed, one particular guide vane is more inclined to vibrate at a higher amplitude than the others. So, at the operating points OP#2, respectively OP#3, the guide vane C, respectively the guide vane B, vibrates with an amplitude more than twice the amplitude of the others.

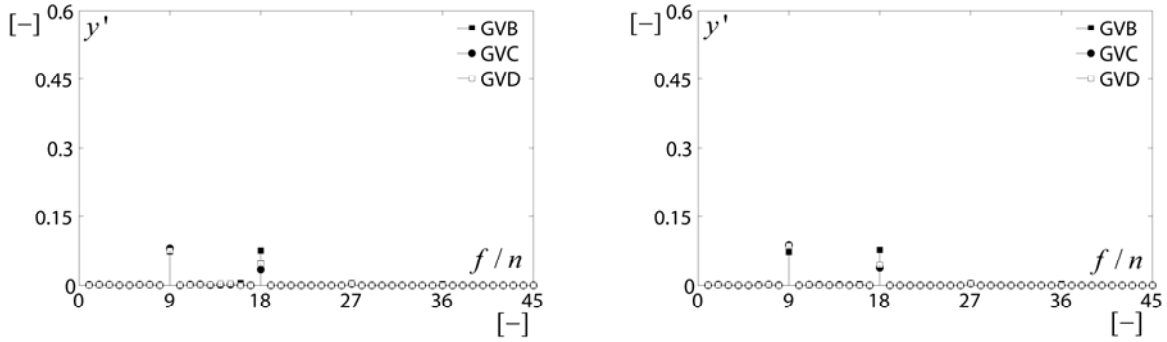

Fig. 5 Relative fluctuating bending displacement for the case of OP#1: config. 1 (left) and config. 2 (right).

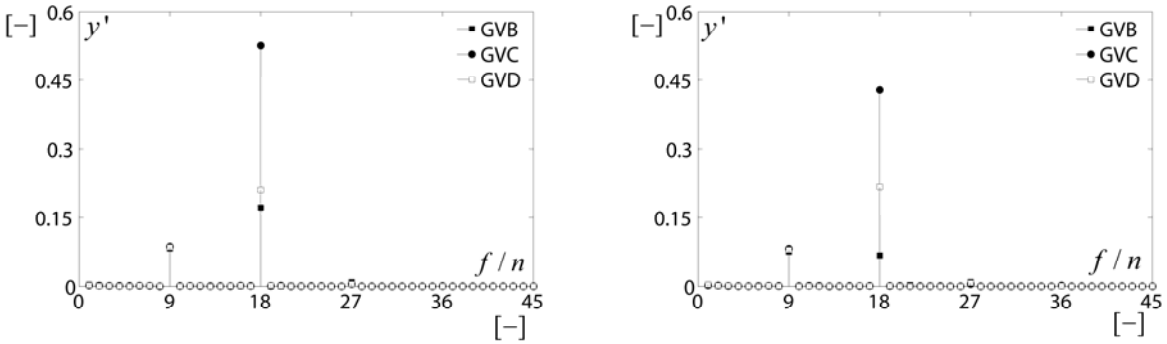

Fig. 6 Relative fluctuating bending displacement for the case of OP#2: config. 1 (left) and config. 2 (right).

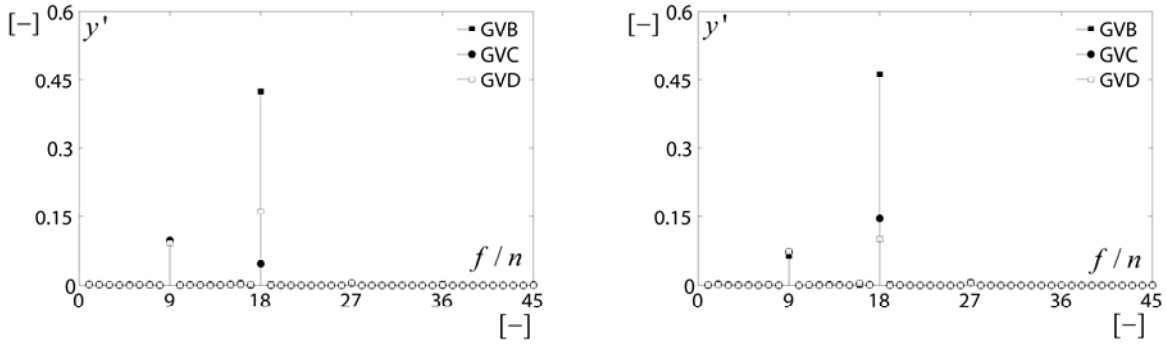

Fig. 7: Relative fluctuating bending displacement for the case of OP#3: config. 1 (left) and config. 2 (right).

As mentioned above, the vibrating guide vanes amplitude has an impact on the flow at the outlet of the inter-stay vanes space. The closest pressure sensor to the guide vane vibrating with the higher amplitude undergoes higher pressure fluctuations. Thus, the pressure sensor 34, respectively 33, monitors higher pressure fluctuations at the operating point OP#2 in the configuration 1, respectively 2 (see Fig. 9), and at the operating point OP#3 in the configuration 2, respectively 1 (see Fig. 10). At the operating point OP#1, the spectra amplitude of sensors 33 and 34 are of the same order of magnitude (see Fig. 8). For the three operating points investigated, the sensors 39 and 40 are not very influenced by the guide vanes vibrations, since they are situated too far from them.

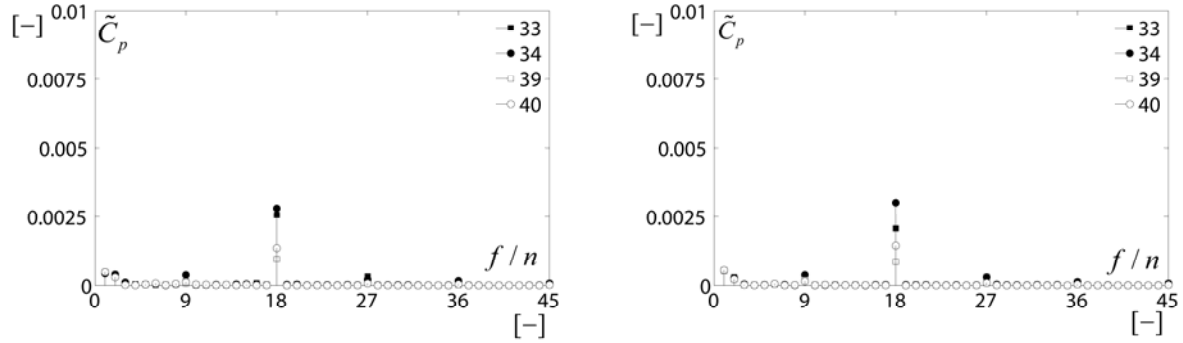

Fig. 8 Pressure coefficient spectra for the case of OP#1: config. 1 (left) and config. 2 (right).

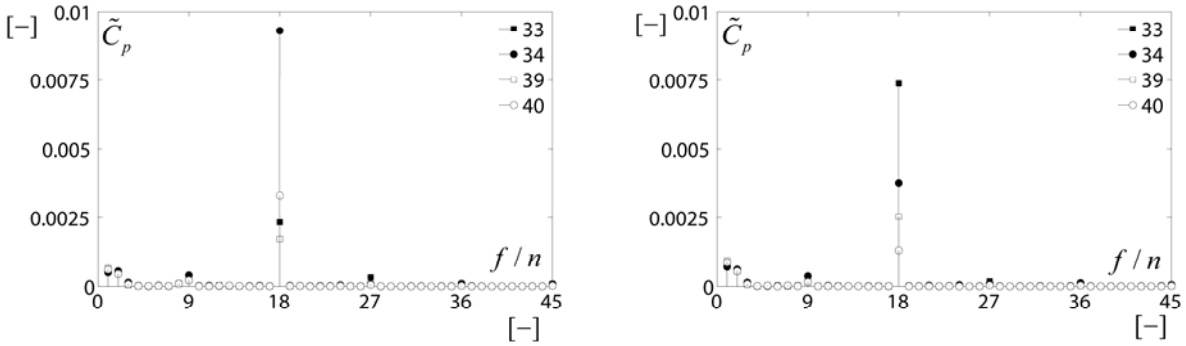

Fig. 9 Pressure coefficient spectra for the case of OP#2: config. 1 (left) and config. 2 (right).

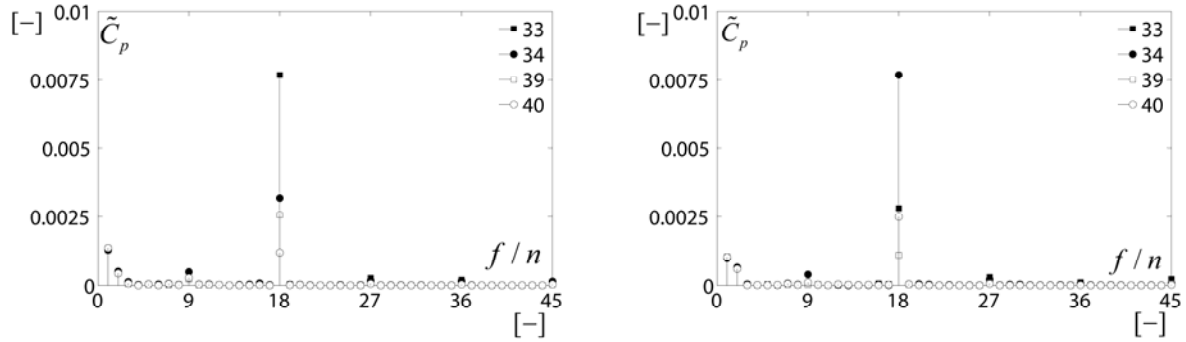

Fig. 10 Pressure coefficient spectra for the case of OP#3: config. 1 (left) and config. 2 (right).

4.2. Flow influence on the structural vibration

To study the flow influence on the vibrating structure when operating the hydraulic pump-turbine, additionally to the rotor-stator interaction excitation, the spark plug is used to give an impulse excitation to the guide vanes. In this way, the guide vanes eigen modes are excited at a higher level than if they are only excited by the flow turbulence and the rotor-stator interaction. The two latter excitation types are called external excitation in the following lines. Two main difficulties are encountered. On the one hand, the head has an influence on the impulse excitation energy. The accuracy and completeness of the modal information is strongly related to the amplitude of the impulse excitation compared to the amplitude of the external excitation. On the other hand, the rotor-stator interaction excitation perturbs the treatment of the impulse response signal when the fundamental or one of its harmonics is close to a guide vane eigen mode. Even by filtering the signals around the eigen modes, they cannot be treated as pure impulse responses. Results based on the assumption of free vibrations, such as those linked to hydrodynamic damping are thus distorted. Therefore, a judicious choice combining the head and the impeller rotation speed has to be made.

In this section, the focus is on the operating point influence on the hydrodynamic damping. With this aim in view, four operating points at 18° opening angle, including the Best Efficiency Point (BEP) – OP#7, are chosen. Their characteristics are given in Tab. 2. The related velocity triangles at the inlet of the runner are given in Fig. 11. The relative flow velocity angle β is assumed to remain constant for the four operating points, but, in reality, this angle varies. Nevertheless, this assumption gives a good qualitative understanding of the occurring phenomenon. Since the discharge is kept as constant as possible (0.11 m^3/s), the absolute flow velocity angle α varies depending on the operating conditions. The further the operating point from the BEP, the higher the absolute flow velocity angle. In reality, the variation of the angle should be lower than the ideal case presented here. The absolute flow velocity angle is rightfully assumed to be 18° at BEP, since the flow should be aligned with the guide vanes opening angle at this operating point.

Tab. 2 Specifications of the operating points OP#4 to OP#7

	Units	OP#4	OP#5	OP#6	OP#7 (BEP)
ϕ	[-]	0.447	0.424	0.397	0.377
ψ	[-]	7.668	6.965	6.303	5.864
α	[°]	27.3	24.0	20.4	18.0
f_p	[Hz]	58.1	61.0	64.0	66.3

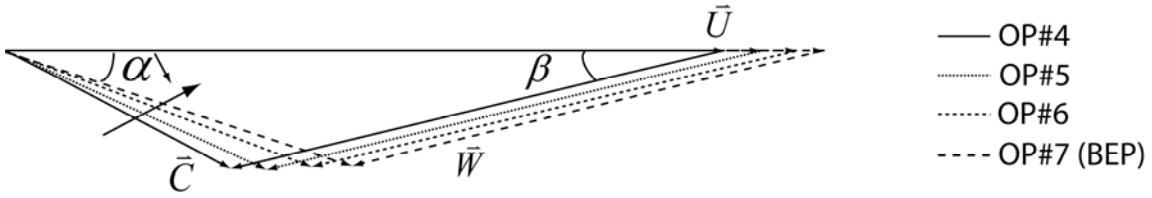

Fig. 11 Velocity triangle related to operating points OP#4 to OP#7

For each of the operating points, 3 acquisitions are made and the hydrodynamic damping values are then averaged on these 3 samples. The vibration signals are digitized at 51.2 kHz sampling frequency over 0.32 s yielding a 3.125 Hz frequency resolution. The hydrodynamic damping λ_f is obtained by fitting the envelope of the impulse response with a decreasing exponential function (see eq.(4)) with amplitude Y' and total damping coefficient $\lambda_{tot} = \lambda_f + \lambda_s$ as parameters (λ_s denotes the structural damping coefficient):

$$\hat{y}'(t) = Y' e^{-\lambda_{tot} t} \tag{4}$$

With this aim in view, the relative fluctuating torque T' acting on the guide vane B at the location GV10 (configuration 2) is first filtered around its torsion eigen frequency at 603 Hz with a Butterworth pass-band filter of degree 3. The filter bandwidth can have an influence on the final value of hydrodynamic damping. The bandwidth is, thus, chosen as large as possible, but the filtered signal must contain only the eigen mode of interest. A bandwidth [560 Hz; 640 Hz] is so chosen. The Hilbert transform is applied to the filtered signal. The signal envelope obtained by taking the norm of the Hilbert transform is then fitted with the decreasing exponential function.

The structural damping coefficient λ_s of the guide vane B is obtained from the impulse response in air over 8 samples and is $\lambda_s = 10.01\ s^{-1}$. The hydrodynamic damping coefficient for each of the operating points is averaged over 3 samples and obtained by subtracting the structural damping coefficient from the total damping coefficient. The values of the hydrodynamic damping coefficient are given in Tab. 3.

Tab. 3 Hydrodynamic damping λ_f for different operating points

	Units	**OP#4**	**OP#5**	**OP#6**	**OP#7**
λ_f	s^{-1}	24.96	21.61	16.44	24.30

The hydrodynamic damping in still flow for the guide vane placed at the GV10 location is determined with the guide vanes configuration 1. So, the structural damping coefficient of the guide vane C is found to be $\lambda_s = 21.05\ s^{-1}$. The total damping coefficient of this guide vane placed at the location GV10 is $\lambda_{tot} = 38.23\ s^{-1}$. This leads to $\lambda_f = 17.18\ s^{-1}$. In still flow, the hydrodynamic damping coefficient is less than for OP#4, OP#5 and OP#7, which is in agreement with the fact that the flow adds hydrodynamic damping. Nevertheless, at the operating point OP#6, the guide vanes located at GV10 undergoes a lower hydrodynamic damping. So, the operating point has an influence on the hydrodynamic damping. Accounting only for the flow velocity around the guide vane leads therefore to a distorted damping prediction. The flow structure as well as the neighboring guide vanes must be considered.

5. Conclusion

In the present paper, fluid-structure coupling is experimentally carried out in the guide vanes cascade of a pump-turbine scale model placed in the EPFL PF3 test rig. An advanced instrumented set is used to monitor the vibrations of 3 adjacent guide vanes and the surrounding flow. The three guide vanes are weakened in order to accentuate the fluid-structure coupling. The paper highlights the interaction between these vibrations and the surrounding flow behavior. On the one hand, the amplitude of the vibrating guide vanes is shown to have a direct impact on the pressure fluctuations amplitude in the inter-stay vanes region upstream from the vibrating guide vanes. On the other hand, the operating point is shown to have an influence on the structure vibrations. Depending on the operating point, the hydrodynamic damping is indeed modified, due to different flow structure. This flow structure change is illustrated in the present paper with the modification of the absolute flow velocity angle at the runner inlet.

Further investigations should lead to a model describing the physics of the guide vanes cascade. In an industrial perspective, the model should be transposed from scale model to prototype.

Acknowledgments

The present investigation was carried out in the frame of HYDRODYNA II project (Eureka N° 4150), in a partnership with ALSTOM Hydro, ANDRITZ Hydro, VOITH Hydro and UPC-CDIF. The authors would like to thank the Swiss Federal Commission for the Technology and Innovation (CTI) and Swisselectric Research for their financial support as well as the HYDRODYNA II partners for their involvement and support.

Nomenclature

C	Absolute flow velocity [m/s]	Y'	Initial amplitude of the envelope $\hat{y}'$ [-]
$\tilde{C}_p$	Pressure coefficient [-]	y'	Relative fluctuating bending displacement [-]
E	Young modulus [GPa]	$\overline{y}$	Bending displacement time average [m]
E	Specific energy [J/kg]	$\hat{y}'$	Envelope of y' filtered [-]
f	Frequency [Hz]	W	Relative flow velocity [m/s]
f_p	Impeller blade passage frequency [Hz]	ρ	Structure density [kg/m^3]
F	Bending force [N]	α	Absolute flow velocity angle [°]
F'	Relative fluctuating bending force [-]	β	Relative flow velocity angle [°]
$\overline{F}$	Bending force time average [N]	ϕ	Pump-turbine discharge coefficient [-]
K	Bending stiffness [N/m]	λ_f	Hydrodynamic damping coefficient [1/s]
p	Fluid pressure [Pa]	λ_s	Structural damping coefficient [1/s]
p'	Relative fluctuating fluid pressure [-]	λ_{tot}	Total damping coefficient [1/s]
$\overline{p}$	Fluid pressure time average [Pa]	ψ	Pump-turbine energy coefficient [-]
Q	Discharge [m^3/s]	σ	Damping coefficient standard deviation [1/s]
U	Impeller circumferential velocity [m/s]	$\sigma_{elastic}$	Elastic limit [MPa]
y	Bending displacement [m]		

References

[1] Bouschon M, Roulet D, Miscioscia T and Pépin P 2008 Recent achievements in hydro actuators *Hydro 2008 Proc.* (Ljubljana, Slovenia)
[2] Miyakozawa T, Kielb R E and Hall K C 2009 The effects of aerodynamic asymmetric perturbations on forced response of bladed disks *J. of Turbom. ASME*
[3] Yan Y J, Cui PL and Hao H N 2008 Vibration mechanism of a mistuned bladed-disk *J. of sound and vibration* **317** 294-307
[4] Brennen C E 1982 *A review of added mass and fluid inertial forces* (Naval Civil Engineering Laboratory, Port Hueneme, California, US, Report CR 82.010)
[5] Kaminer A A and Kavitskii B M 1976 Experimental investigation of hydrodynamic damping during bending oscillations of blade profiles in water flow *Strength of Materials* 25-7
[6] Theodorsen T 1935 *General Theory of Aerodynamic Instability and the Mechanism of Flutter* (NACA Report 496)
[7] Roth S, Calmon M, Farhat M, Muench C, Huebner B and Avellan F 2009 Hydrodynamic Damping Identification from an Impulse Response of a Vibrating Blade Proc. of the *3rd IAHR Int. Meet. of the Workg. on Cavit. and Dyn. Probl. in Hydr. Machin. and Syst.* (Brno, Czech Republic) **1** 253-70
[8] Münch C, Ausoni Ph, Braun O, Farhat M and Avellan F 2008 Hydro Elastic Behavior of Vibrating Blades *Proc. of the 24th Symp. on Hydr. Machin. and Syst.* (Foz do Iguassu, Brazil)
[9] Zobeiri A, Kueny J L, Farhat M and Avellan F 2006 Pump-Turbine Rotor-Stator Interactions in Generating Mode: Pressure fluctuation in Distributor Channel *Proc. of the 23th Symp. on Hydr. Machin. and Syst.* (Yokohama, Japan)
[10] Roth S, Hasmatuchi V, Botero F, Farhat M and Avellan F 2010 Advanced Instrumentation for Measuring Fluid-Structure Coupling Phenomena in the Guide Vanes of a Pump-Turbine Scale Model *Proc. of the ASME 2010 7th Int. Symp. on Fluid-Struct. Interact., Flow-Sound Interact., and Flow-Induced Vibrat. & Noise* (Montreal, Canada)
[11] Pereira F, Farhat M and Avellan F 1993 Dynamic calibration of transient sensors by spark generated cavity *Proc. of IUTAM Symp. on Bubble Dynam. and Interf. Phenom.*